Natural goethite reduced with dithionite: Evaluation of the reduction process by XANES and Mössbauer spectroscopy and application of the catalyst in the oxidation of model organic compounds

Anelise L. de Abreu, Iara R. Guimarães, Alexandre dos S. Anastácio [1], Mário C. Guerreiro *

Department of Chemistry, Federal University of Lavras, P.O. Box 3037, CEP 37200-000 Lavras, MG, Brazil

ARTICLE INFO

ABSTRACT

Iron oxides have been used as catalyst in different industrial applications, prominently in the petrochemical field. Natural goethites are interesting materials since they have a high surface area compared to their synthetic counterparts and also have a high relative abundance in the environment. Chemical treatment with sodium dithionite may cause surface changes of the goethite improving its catalytic activity. In this work, a natural goethite was used after dithionite treatment in the catalytic oxidation of methylene blue and quinoline. Infrared spectroscopy (FTIR) and temperature programmed reduction (TPR) were utilized for characterization. Quinoline oxidation by-products were monitored by electrospray mass spectroscopy (ESI-MS). After treatment, hydrogen peroxide decomposition was enhanced, indicating a radical mechanism. The same mechanism can be ascribed for the catalytic oxidation of quinoline since hydroxylation intermediates were observed. The same kind of mechanism can also be proposed for the methylene blue oxidation.
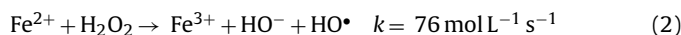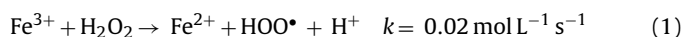
1. Introduction

Currently, catalysts based on iron oxide are widely used in Fenton type processes as an alternative for the treatment of several organic classes of polluting effluents [1–4]. Among those oxides, goethite (ideal formula α-FeOOH) is one of the phases that have been studied extensively due to its high catalytic activity, allied to a significant thermodynamic stability [5].

Goethite is the first oxyhydroxide to be formed under ambient conditions. It is naturally found in various soils and sediments, most of the time presenting a low crystallinity and a yellow or brownish color [2,6]. Some peculiar properties of the natural goethites, such as a high surface area (for example 65 $m^2 g^{-1}$ [7] for natural goethite and area ranging from 8 to 22 $m^2 g^{-1}$ for goethites prepared using different synthesis methods [8]), have been promoting a growing interest in the use of this mineral, above all, in catalytic processes of interest to the industrial sector [9], and advanced oxidative processes, such as Fenton type systems [1,2,6].

Reactions involving the formation of hydroxyl radicals catalyzed by iron oxides in heterogeneous medium have been receiving special attention due to the advantages in relation to the classic homogeneous process (Fenton process). Some of these advantages are: (i) easiness in the separation of the catalyst after treatment of the effluent; (ii) absence of the acidification stage (for pH 3) and subsequent neutralization, thus avoiding sludge generation and (iii) capacity of the catalyst to be recycled/regenerated [10].

The generation of radicals catalyzed by an iron phase such as goethite, in which iron (III) and hydrogen peroxide are present, can be described by Eqs. (1) and (2):

$$Fe^{3+} + H_2O_2 \rightarrow Fe^{2+} + HOO^\bullet + H^+ \quad k = 0.02 \, mol \, L^{-1} \, s^{-1} \tag{1}$$

$$Fe^{2+} + H_2O_2 \rightarrow Fe^{3+} + HO^- + HO^\bullet \quad k = 76 \, mol \, L^{-1} \, s^{-1} \tag{2}$$

The reaction between the Fe^{3+} site of the goethite and hydrogen peroxide forms a hydroperoxyl radical and Fe^{2+} (Eq. (1)). The hydroxyl radical is formed in the reaction of Fe^{2+} and hydrogen peroxide [3,11–13] (Eq. (2)). This can attack the pollutant organic compounds present in the reaction medium, oxidizing them to intermediates and achieving, sometimes, total mineralization [6,14].

The catalytic decomposition of the peroxide in the presence of iron (II) is more advantageous, because that reaction type, besides being faster, leads to the direct formation of hydroxyl radicals (Eq. (2)), while in the presence of iron (III) (Eq. (1)), the formation of the hydroperoxyl radical occurs first ($E^o = 1.70 \, V$), which presents a low oxidation potential compared the hydroxyl radical ($E^o = 2.80 \, V$) and therefore is less efficient in the oxidation of organic pollutants [15].

The chemical treatment of minerals with dithionite was used initially for the selective removal of iron in soil samples [16]. Such method was modified for the reduction of the structural iron in clay minerals [17], but has the disadvantage of requiring an inert atmosphere during the reduction and using deaerated solutions and oxygen-free water.

Dithionite, in aqueous solution, undergoes disproportionation into thiosulfate and sulfite (Eq. (3)) or it can even suffer a direct monomerization reaction, forming sulfoxylate radicals (Eq. (4)).

$$2S_2O_4^{2-} + H_2O \rightarrow S_2O_3^{2-} + 2SO_3^- + 2H^+ \tag{3}$$

$$S_2O_4^{2-} \rightleftharpoons 2SO_2^{-\bullet} \tag{4}$$
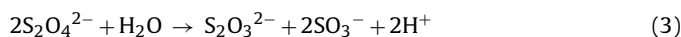
It is exactly the activity of this free radical which is responsible for the reduction of dithionite [18].

The treatment with dithionite can represent a relatively simple and cheap method for the activation of catalysts, since the resulting structures present larger structural defects and, therefore, they can work as active catalytic sites [19]. In this study the effect of the chemical treatment with sodium dithionite was evaluated on the structural and catalytic properties of a natural goethite, using the model molecules methylene blue and quinoline. The oxidation products were monitored by electrospray ionization mass spectrometry (ESI-MS).

2. Experimental

2.1. Preparation of the materials

The natural goethite was treated with dithionite according to the method described by Mehra and Jackson [16]. Portions of 1.0 g of natural goethite were resuspended for subsequent reduction by mixing with 20 mL of 0.3 mol L^{-1} sodium citrate solution (Na$_3$C$_6$H$_5$O$_7$·2H$_2$O) and 5 mL of 1 mol L^{-1} sodium bicarbonate solution (NaHCO$_3$) in a 100 mL polypropylene centrifuge tube. 1 g of sodium dithionite (Na$_2$S$_2$O$_4$) was then added. The citrate–bicarbonate buffer was used in order to maintain a near-neutral pH and thereby minimize acid dissolution during treatment with Na$_2$S$_2$O$_4$. Using a glass rod the material was agitated for 1 min and the tube maintained under heating and mechanical agitation in a water bath between 75 °C and 80 °C, under anaerobic conditions. Another 1 g of sodium dithionite was added and the agitation continued for 15 min in the water bath between 75 °C and 80 °C to complete the reaction. After this the mixture was centrifuged for approximately 5 min at 1300 × g and washed three times with water for total removal of the bicarbonate. The solid fraction was over dried at 60 °C.

2.2. Catalytic tests

The catalytic activity of the materials was evaluated by decomposition of hydrogen peroxide (H$_2$O$_2$), monitoring the liberated oxygen. 10 mg of the material, 5 mL of distilled water and 2 mL of H$_2$O$_2$ 50% (v/v) were mixed and maintained in an isolated volumetric system. The oxygen liberation was monitored by the increase of the gas column in the volumetric system with a pressure equalizer. To investigate if the peroxide decomposition is a radical process, the experiments were repeated replacing the distilled water by 50 mg L^{-1} solutions of methylene blue (MB) or quinoline.

The degradation tests of methylene blue and quinoline were conducted using 9.9 mL of a solution at a concentration of 50 mg L^{-1}, 0.1 mL of H$_2$O$_2$ 50% and 10 mg of the catalyst, under constant agitation at 100 rpm, using reaction times of 0, 60, 120, 180 and 240 min. The adsorption kinetics was followed in a UV–vis spectrometer (SP-2000 UV). The temperature used in the tests was 25 °C ± 1 °C. The products of quinoline and MB degradation were

monitored by electrospray ionization mass spectrometry in a positive mode (ESI-MS Agilent-1100) in an attempt to identify the intermediates. The reaction was analyzed by direct infusion with a flow rate of 15 μL min^{-1} and the spectra were obtained as an average of 50 scans. The injection conditions were: temperature 320 °C and 12 psi pressure, capillary voltage 3.5 kV, skimmer voltage 35 V, capillary exit 125 V, target mass adjusted to 300 and ICC 30000 with a maximum accumulation of 300 ms. Nitrogen was used as the drying gas with a flow rate of 6 L min^{-1}. The resulting product ion spectra were highly reproducible. For ESI-MS/MS, the parent ion of interest was first isolated by applying an appropriate waveform across the end cap electrodes of the ion trap to resonantly eject all trapped ions, except those ions with m/z ratio of interest. The isolated ions were then subjected to a supplementary AC signal, to resonantly excite them causing collision-induced dissociation (CID) using helium.

2.3. Caracterization of the materials

2.3.1. Infrared spectroscopy (FTIR)

The infrared spectra were obtained in a Digilab Excalibur spectrometer, FTS 3000 series, 400–4000 cm^{-1} spectral range and 4 cm^{-1} resolution, using KBr pellet.

2.3.2. Temperature programmed reduction (TPR)

The temperature programmed reductions (TPR) (Chembet 3000, Quantachrome) were carried out by monitoring the hydrogen consumption through a thermal conductivity detector. About 50 mg of each sample were heated under a flow of 20 mL min^{-1} H$_2$ (5%)/N$_2$ at a rate of 5 °C min^{-1} from room temperature to about 1000 °C.

2.3.3. Mössbauer spectroscopy

Mössbauer spectroscopy was used to study the distribution of the iron phases in the material before and after the dithionite treatment. The samples were diluted and triturated with sucrose to obtain 10 mg cm^{-2} of iron. The Mössbauer spectra were obtained at room temperature, using a spectrometer with transducer and CMTE model MA250 function generator, and a ^{57}Co/Rh source. The samples were prepared in pellets, used as absorbers. The isomeric displacement of the samples was referenced by calibration using a metallic iron leaf (α-Fe).

2.3.4. XANES spectral collection

X-ray absorption measurements were carried out in the facility of the Brazilian Synchrotron Light Laboratory (LNLS–Campinas – Brazil) with synchrotron radiation using the Fe K-edge XANES spectra minimum of three spectra were collected of each sample. LNLS operates at 1.37 GeV and 250 mA. Energy selection was achieved with silicon channel-cut monochromators, and we tested on both Si (3 1 1) and Si (1 1 1) lattice cuts. The improvement in spectral resolution was obtained using a Si (3 1 1) relative to a (1 1 1) crystal. The specifications provided below apply to the Si (3 1 1) monochromator and all data presented in this study were collected using the Si (3 1 1). The first derivative peak for α-Fe, set to 7112 eV, defines the energy calibration for the system.

3. Results and discussion

3.1. Characterization of the materials

3.1.1. Infrared spectroscopy

The infrared spectrum (not shown) of natural goethite presents characteristic O—H stretching bands, in which the higher frequency (3500 cm^{-1}) band is attributed to surface hydroxyls and the lower frequency band (3170 cm^{-1}) to internal hydroxyls. Furthermore, the O—H stretching small bands at 3701 cm^{-1} and a shoulder at
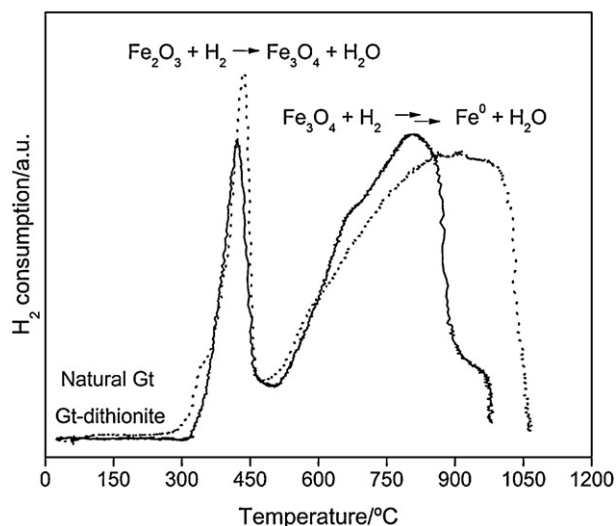
Fig. 1. Temperature programmed reduction of the materials.

Fig. 2. Mössbauer spectrum of the natural goethite at room temperature and at 20 K.

$1622 \, cm^{-1}$ that can be attributed to the presence of kaolinite. The band at $1034 \, cm^{-1}$ (Si—O bond stretching) also confirms the presence of silicate. The bands at $905 \, cm^{-1}$ and $800 \, cm^{-1}$ are due to the planar and out of plane deformations of goethite hydroxyls and are characteristic for this phase [5]. The IR band at $630 \, cm^{-1}$ can be assigned to Fe–O stretching vibrations.

After the treatment with dithionite, the bands corresponding to kaolinite show increased intensities, indicating that a partial dissolution of the iron oxide has taken place. For the treated goethite, no change of the vibration frequency can be observed. According Cornell and Schwertmann [5] this behavior was expected since this effect becomes a weak for the amorphous or poorly crystallinity samples.

3.1.2. Temperature programmed reduction (TPR)

The reduction properties of the goethites were studied by TPR analyses. Fig. 1 shows the TPR profile for natural and reduced goethite–dithionite samples. The TPR profile of the reduced natural goethite is relatively similar to that of the natural goethite (Fig. 1), showing two regions of H_2 consumption. The first H_2 consumption signal is close to $420\,°C$ due to the reduction of the recently formed hematite (ideal formula α-Fe_2O_3 for the goethite dehydroxylation) to magnetite (Fe_3O_4) [16]. The second H_2 consumption area represents the multiple transitions of the magnetite to metallic iron.

The treatment with dithionite reduces the stability of the material because both reduction signals are slightly moved towards lower temperatures. The natural goethite reduces at $435\,°C$ while the treated material – Gt–dithionite – begins the reduction process at $420\,°C$. The integration of the reduction peaks (by the Lorentz Model) indicates a loss of about 24% after the treatment, which indicates the partial reduction of iron (III) on the catalyst surface by the dithionite treatment. This result was verified by IR spectroscopy (not shown, available in Supplementary material). Previous studies indicate that dithionite is able to reduce Fe^{3+} to Fe^{2+} when accompanied with a CO_3^{2-}/HCO_3^- buffer, and that the reaction occurred via Eq. (5):

$$S_2O_4^{2-} + 2Fe^{3+} + 2H_2O \rightarrow 2SO_3^{2-} + 2Fe^{2+} + 4H^+ \qquad (5)$$
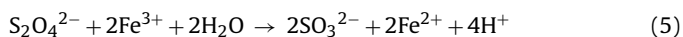
It should be noted that the dithionite ion is in equilibrium with sulfoxylate radicals as shown by Eq. (4).

3.1.3. Mössbauer spectroscopy

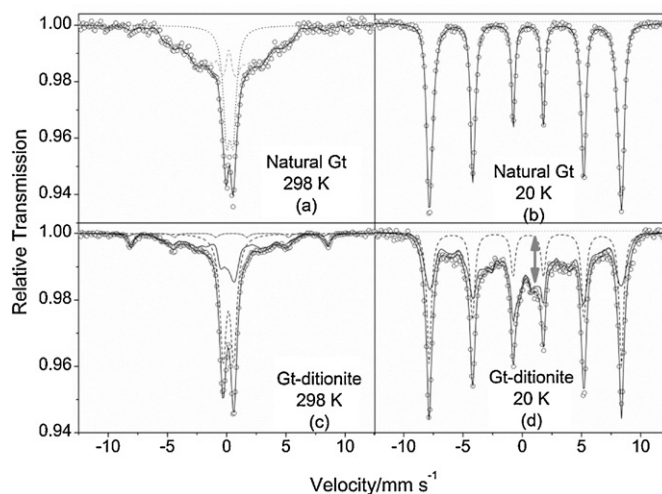The Mössbauer spectrum of the natural goethite at room temperature (Fig. 2) is dominated by a quite relaxed and badly defined sub-structure due to the small size of the goethite particles. Moreover, there is a central doublet characteristic for a paramagnetic component and responsible for 34% of the total area. When the temperature was lowered to 20 K (Fig. 2), a complete magnetic ordering occurred, since only a characteristic sextet is observed. The hyperfine parameters data obtained from the Mössbauer analysis indicate that the goethite is the only phase present, with B_{hf} 51.9 T.

After dithionite treatment, the Mössbauer spectrum at room temperature (Fig. 2) presents an increase of the central doublet, indicating that there was an increase in the prevalence of goethite with small particle sizes (51% of total area). Moreover, the relative increase in the area regarding the presence of the goethite phase can be derived from the leaching of iron species dispersed or loosely bound to the mineral structure. Goethite treated with dithionite shows an adjustment with a sextet with hyperfine field that indicates the presence of a reduced iron phase, such as magnetite. This fact was proven by the measurements at low temperature (Fig. 2) where the poorly defined spectrum gives way to one with a well-defined sextet. The adjustment for the crystalline site and the hyperfine field distribution was made in order to explain the effect of the particle size of the samples. The prevalence of the relaxation in the spectrum, shown in Fig. 2 by double arrow, can be indicative that the treatment concentrates smaller sized crystallites. The values of this hyperfine field for the Gt–dithionite spectrum at 20 K indicate the presence of goethite (predominant phase) and magnetite, possibly located on the catalyst surface due to chemical treatment as shown by the TPR data analysis.

The Mössbauer experimental results explain some aspects of why $Na_2S_2O_4$ reduces more Fe^{3+} in the iron oxide structure. When unpaired electrons are involved in the reducing processes, the following steps may take place:

(i) the active free radicals (e.g., $SO_2^{\bullet-}$) approach the natural goethite surface and transfer electrons to structural Fe^{3+}, reducing it to Fe^{2+};

(ii) because of this initial reduction, the crystalline structure of the iron mineral is energetically destabilized by an excess negative charge, causing partial dehydroxylation and/or other crystalline rearrangements, which, in turn, energetically activate point defects within the crystal. This appearance of defects which is usually accompanied by a decrease in the ordering of the material reflects the relaxation observed after the oxide treatment with dithionite, especially when observing the data obtained at 20 K.
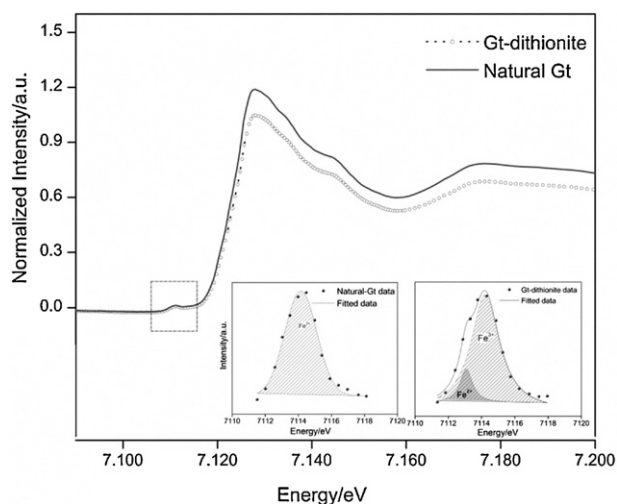
Fig. 3. Normalized spectra of XANES of natural goethite and Gt–dithionite. Inset: extracted pre-edges fitted.

(iii) The excess electrons at point defects may pass to structural Fe^{3+}, which is reduced. The processes continue until all structural Fe^{3+} is reduced [17].

3.1.4. XANES spectroscopy

In Fig. 3 a typical iron Fe–K-edge XANES spectrum of the iron oxide. Is shown at the Fe–K edge XANES spectra features identified as transitions to bound states, either $1s \rightarrow 3d$ (pre-edge) or $1s \rightarrow 4s$ (shoulder) or $1s \rightarrow 4p$ (edge crest) [20]. More precisely, the pre-edge peak is explained by two contributions, due to the Fe^{2+} and Fe^{3+} contents. The pre-edge region is especially sensitive to the oxidation state and to the local environment of iron. Specifically, there is a relationship between the oxidation and coordination states and the position and intensity of the pre-edge, with a higher intensity for tetrahedral than for octahedral sites [21,22]. Low intensities refer to geometries with a center of symmetry (e.g., octahedral); high intensities refer to non-centrosymmetric geometries (e.g., tetrahedral). All attributions were made using pre-edges of model compounds with known Fe-site geometries and oxidation states [23].

According to the data shown in Fig. 3 the pre-edge intensity decreases with the treatment, a variations that may be related to the transition from goethite (Fe^{3+} octahedral) to magnetite phase (a combination between the oxidation states of Fe^{3+} tetrahedral/Fe^{2+} and Fe^{3+} octahedral) (see inset in Fig. 3). In this context the formation of an octahedral coordination environment contributes to decrease in the pre-edge signal. The pre-edges show a structure consisting of two overlapping peaks separated by about 1.5 eV depending on Fe oxidation state. The different relative intensities of the two contributions reflect the different oxidation states of the samples. The pre-edge centroid position depends strongly on the Fe oxidation state, whereas the pre-edge intensity is mostly influenced by the Fe coordination geometry [23]. For sample goethite–dithionite, about 12% of the iron species present in the compound are in the bivalent form while the remaining 88% are related to the presence of trivalent iron. It is important to note here that the analysis now focuses on the oxidation state is not the environment of coordination. It is important to note here that the analysis focuses on the iron oxidation state and not on the environment of coordination of the iron (III). Thus the total iron (III) content is the sum of Fe^{3+} present in tetrahedral and octahedral coordinations of magnetite and
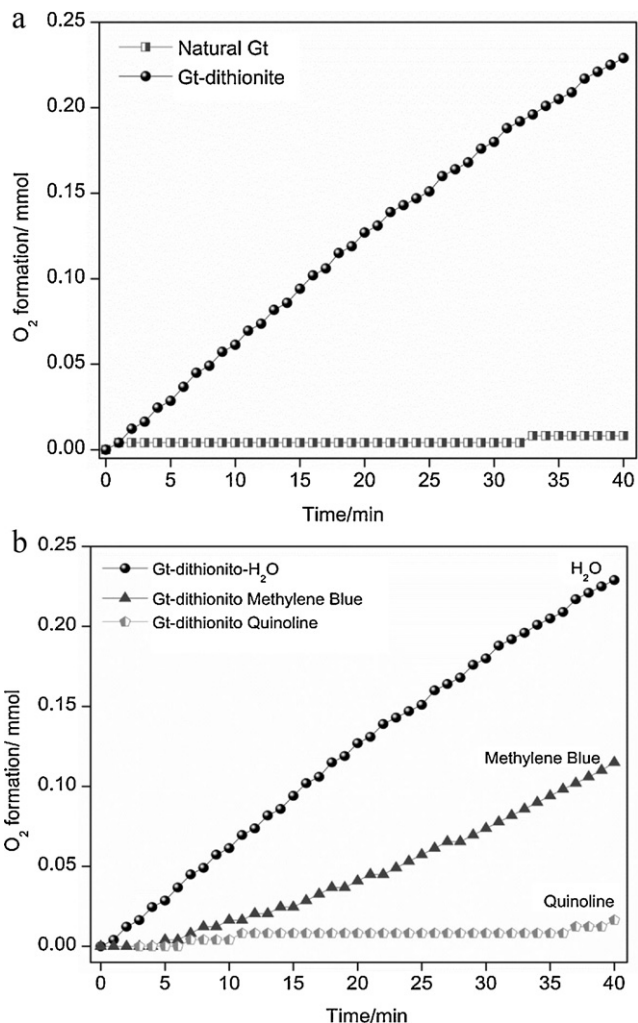

Fig. 4. Decomposition of hydrogen peroxide in the presence of natural goethite and natural goethite treated with dithionite in aqueous (a) and organic medium: methylene blue and quinoline ($50 \, mg \, L^{-1}$) (b).

goethite, respectively. The differences between these spectra thus indicate that redox reactions can be monitored through XANES spectroscopy and that the observed variations of the spectra allow redox changes to be determined as a function of chemical modification.
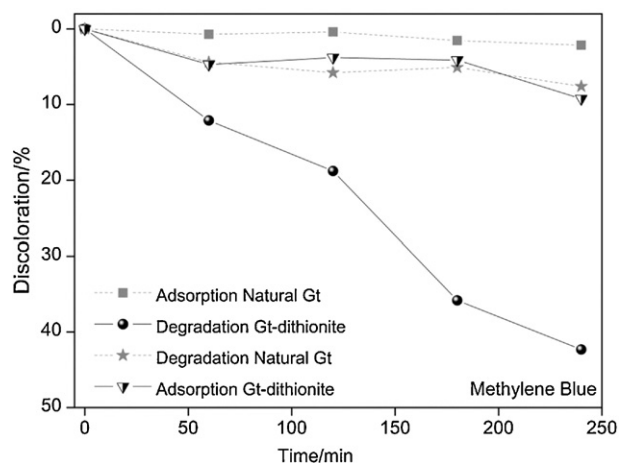

Fig. 5. Adsorption kinetics and methylene blue degradation ($50 \, mg \, L^{-1}$) in the presence of natural and dithionite treated goethite.
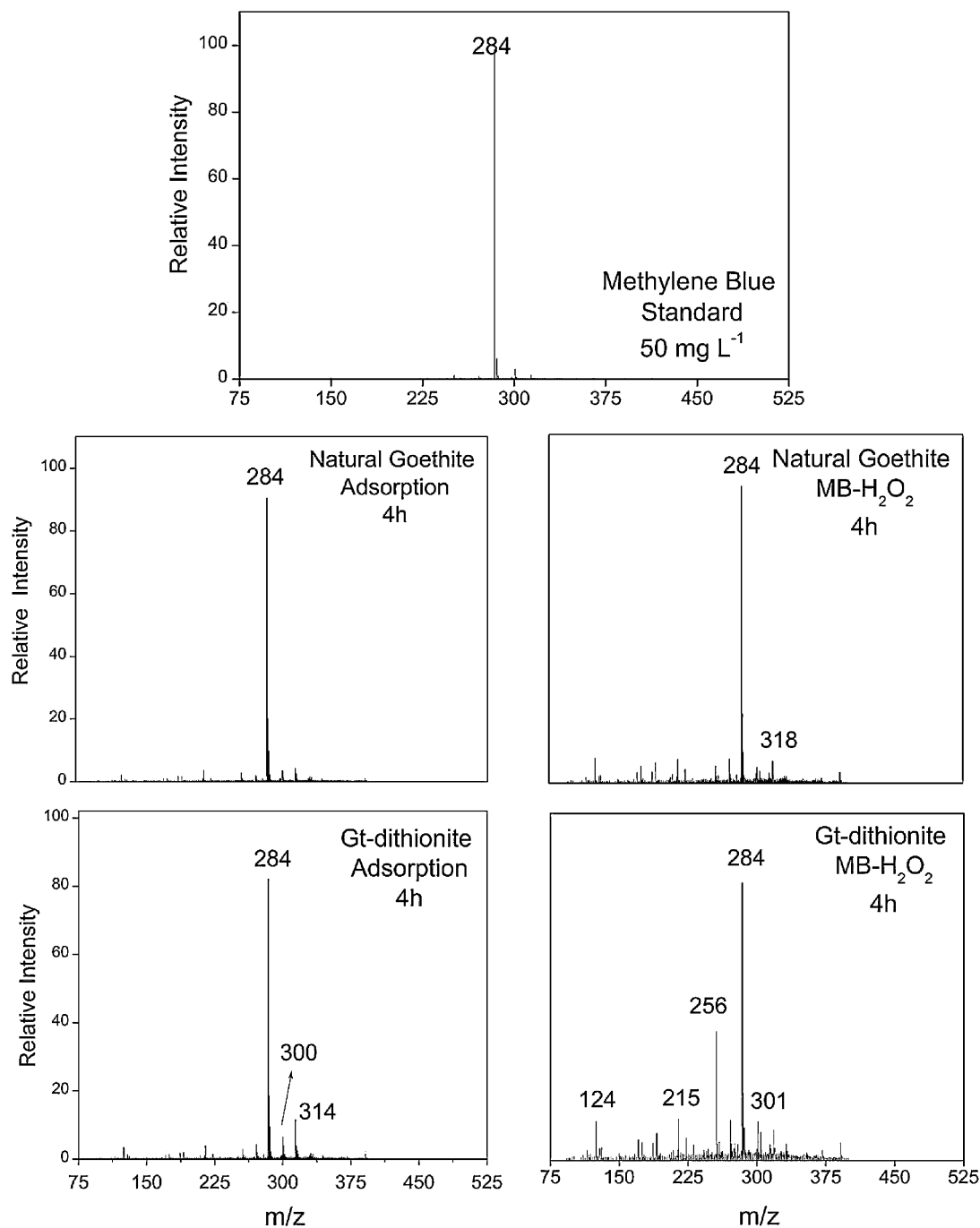
**Fig. 6.** Mass spectra of the standard methylene blue solution in goethite samples.

3.2. Catalytic tests

3.2.1. H_2O_2 decomposition

The decomposition of H_2O_2 has long been a subject of interest, especially because H_2O_2 has been used as a source of hydroxyl radicals, an oxidant in the degradation of organic pollutants from water, as well as for the oxidation of some other compounds [21]. The mechanism of the Fenton-like oxidation process includes radical intermediates from hydrogen peroxide decomposition (e.g., $HO^\bullet$) and scavenging reactions [22]. In publications the catalyst activity was reported to be proportional to its ability to decompose hydrogen peroxide. So the decomposition of H_2O_2 in the presence of different goethite samples is showed in Fig. 4a. The kinetics of hydrogen peroxide decomposition in water, catalyzed by natural and treated goethites, evidence that the treatment with dithionite significantly improves the activity of the material. This increase in capacity of radical formation is directly related to the presence of reduced iron species – Fe^{2+} – [24,25] on the catalyst surface after chemical treatment, as suggest by Mössbauer and TPR analyses.

Furthermore, the presence of methylene blue in the reaction mixture inhibits oxygen formation, indicating that the hydrogen peroxide decomposition is preferentially a radical process [12]. In the presence of quinoline the same behavior is observed (Fig. 4b). In other words, the treatment with dithionite increases the decomposition capacity for the peroxide and the presence of the organic inhibits the formation of oxygen, evidencing the radical process of the reaction [12].
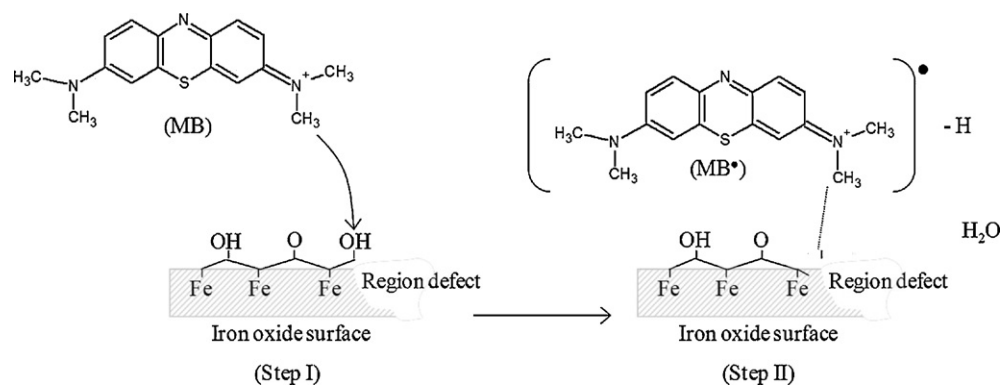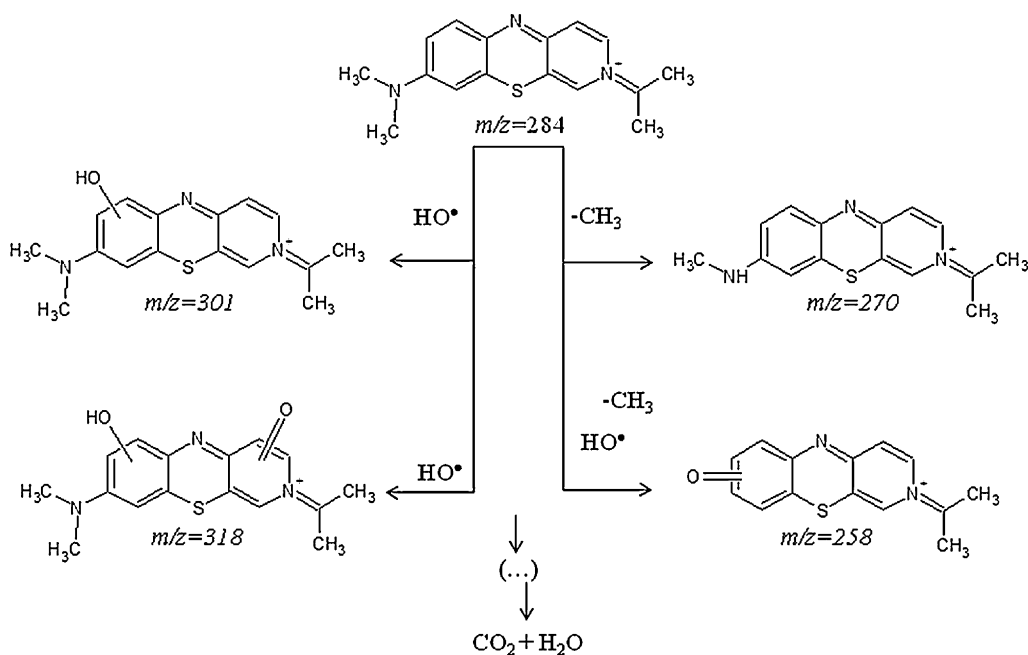
Scheme 1.

Fig. 7. Possible intermediates formed in the methylene blue oxidation.

3.3. Adsorption and oxidation of methylene blue

The adsorption and oxidation of MB for the surface of iron oxides were investigated in this study. The results are showed in Fig. 5. The removal of methylene blue from the solution by adsorption on natural goethite was insignificant, reaching a maximum of 2% of discoloration. Likewise, the oxidation process also presented a low removal percentage, with a maximum of 8%. The low catalytic activity of the natural goethite can be attributed to the iron phase, constituted by Fe^{3+} species, which presents a much lower peroxide decomposition rate, when compared to other iron phases [15]. This result corroborates with those obtained in the peroxide decomposition in which a radical mechanism was proposed.

Little reduction of MB (less than 9%) was observed in the presence of goethite treated with dithionite. The oxidation process showed the greatest catalytic effect of this material on MB degradation, causing a color reduction of approximately 42% after 4 h of reaction. The increase of the methylene blue removal capacity indicates that the chemical treatment was efficient in increasing of the catalytic capacity. This effect can be associated to the creation of structural defects, which, in a certain manner, increase the number of active sites for the hydroxyl radical formation, as

previously proposed [22,24–27]. No significant liquid-phase reaction was observed.

The confirmation of the radical oxidation mechanism of MB as well as the attempt to identify the oxidation intermediates was carried out through ESI-MS studies in the presence of natural goethite and of dithionite treated goethite. The mass spectra of the standard methylene blue solution only present a mass/charge signal at 284, characteristic for that molecule (Fig. 6). After 4 h in contact with both materials, the methylene blue solution still presents the intense signal at $m/z = 284$ which refers to the methylene blue molecular ion. Comparing, the relative intensity of the mass/charge signal of methylene blue in contact with the materials, it can be verified that the intensity of the solution in contact with dithionite treated goethite was lower, which suggests the occurrence of reactions on the surface of the oxide. Treatment with dithionite possibly led to the formation of defects in regions with high reactivity, which is responsible for the emergence of intermediaries even in the absence of oxidant. In this process natural goethite is less evident, suggesting a reactive surface after chemical reduction.

This is an indication that the treatment with dithionite increases the adsorption capacity possibly by the mechanism reported by other authors in a particular process known as reactive adsorption [26]. It is believed that in this process the molecules are adsorbed
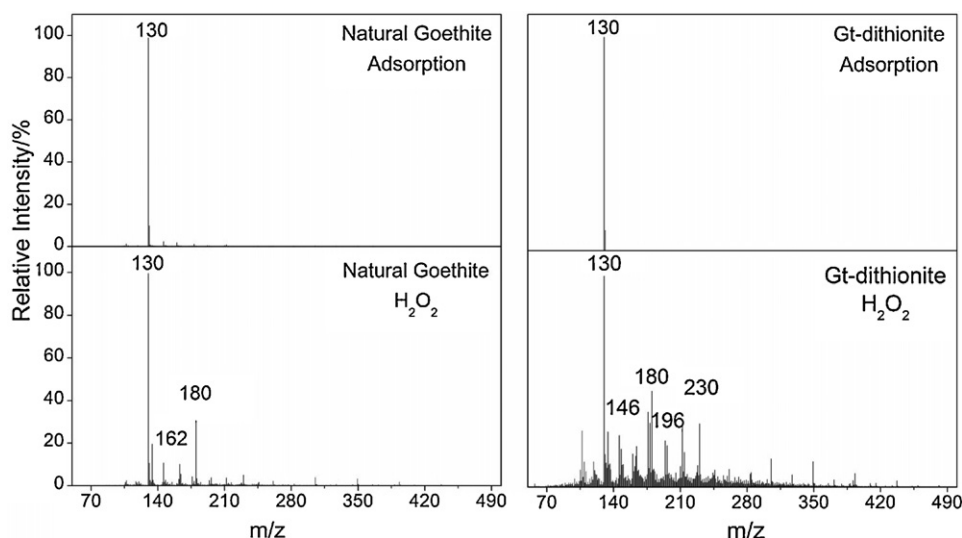
Fig. 8. Mass spectra of quinoline after 24 h in natural goethite and natural goethite treated with dithionite, the quinoline oxidation reactions after 24 h with H_2O_2 in the presence of natural goethite and natural goethite with dithionite. Intensity normalized with respect to the signal m/z of greater intensity in each analysis.
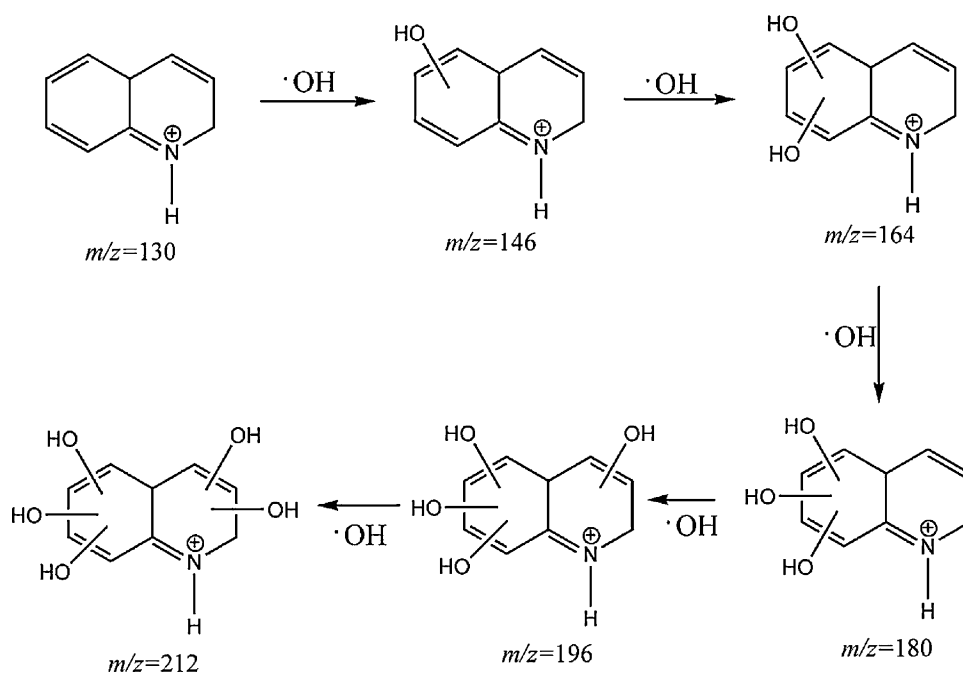

Fig. 9. Formation of possible intermediates formed in the quinoline oxidation.

on oxide surfaces through reaction with hydroxyl groups resulting in H_2O elimination (Scheme 1 – Step I). A methylene blue molecule adsorbed on a goethite site results in the formation of a MB-radical (MB$^•$) (Step II). This highly reactive species (MB$^•$) is able to abstract a hydrogen from water molecules to form hydroxyl radical type, which can now attack the dye molecule itself.

The methylene blue degradation products were monitored by ESI-MS (Fig. 6). The mass spectrum after the degradation reaction shows the presence of new m/z signals at 124, 215, 256 and 301. These reaction intermediates correspond to hydroxylation reactions (m/z at 301), demethylation reactions of the lateral chain and hydroxyl radical attack on the demethylated intermediates. Despite of the catalyst cited by Souza et al. [27] presenting higher activity compared to the treated natural goethite the use of formic acid is the main drawback of the goethite/formic acid system as the organic acid is highly toxic and it very hard to recover at end

of reaction. Structures resulting from the rupture of the aromatic rings were also detected. Based on these new m/z signals detected, a reaction scheme can be proposed for the oxidation of the methylene blue by the goethite treated with dithionite (Fig. 7).

3.4. Adsorption and oxidation of quinoline

The quinoline adsorption kinetics was monitored by UV–vis spectrometry in the presence of natural and treated goethite in order to verify their contribution to the oxidative degradation process. The removal of the quinoline from the solution by adsorption was slightly superior for the dithionite treated goethite, which was 17% for the treated material and 10% for the natural goethite, UV–vis measurements (not shown, data available in Supplementary material). This indicates that the treatment improves the immobilization of organic compounds on its surface. Furthermore, the
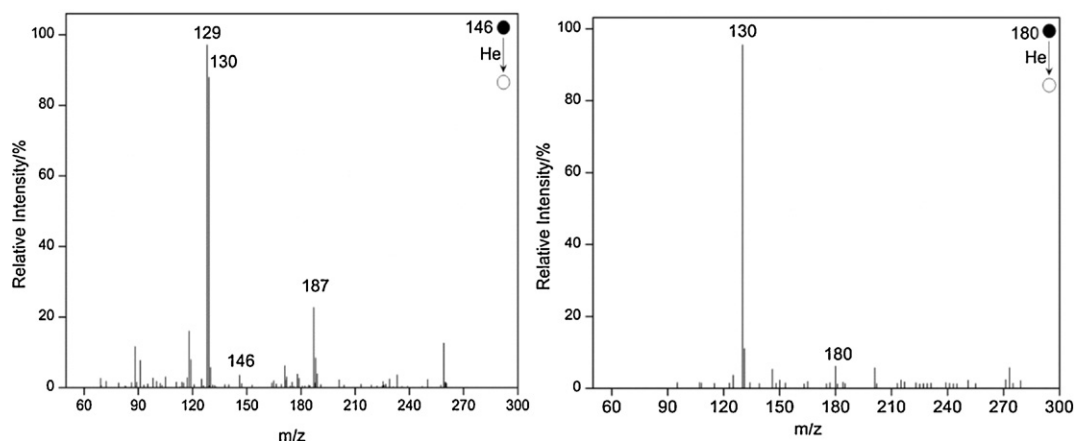
Fig. 10. Product ion ESI-MS/MS mass spectrum for CID of the ion of m/z 146 and 180.

adsorption process seems to facilitate the degradation of the quinoline. The same effect was observed for methylene blue.

The catalytic oxidation of quinoline (ion type M+H$^+$, with $m/z = 130$, $129 + H^+$) was monitored by electrospray ionization mass spectrometry (ESI-MS). It was first verified if the surface of the materials would be capable of reacting with the quinoline. After 24 h of adsorption both materials only presented quinoline in the solution. The higher adsorptive capacity of the treated goethite was again proven, when the intensities of the signals corresponding to quinoline of this material are compared with the natural goethite (Fig. 8).

After 24 h of oxidation reaction, the natural goethite presented ions with m/z at 180 and 196, which correspond to the entrance of three and four hydroxyls in the quinoline structure, respectively (Fig. 8). Analyzing the mass spectrum of the goethite treated with dithionite, it can be verified that other hydroxylations occurred, with the entrance of hydroxyls. Moreover, a comparison among the intensities of the signal at $m/z = 130$, shows that the chemical treatment with the dithionite was more efficient for the removal of the quinoline from the reaction mixture, since the intensity of this ion was about 36% less than that observed in the natural goethite reaction (intensity normalized with respect to the base peak in each analysis, absolute intensities of the base peak: $m/z_{130\ Quinoline\ standard} = 9,101,700$; $m/z_{13\ Natural\ goethite} = 3,933,534$ and $m/z_{130\ Gt\text{-}dithionite} = 596,480$).

Based on these new m/z signals, a reaction pathway with possible intermediates can be proposed for quinoline oxidation by goethite treated with dithionite (Fig. 9) [21].

Under the applied ESI-MS/MS experimental conditions for quinoline, nearly all the fragment ions can be interpreted as dehydroxylation fragment ions with a single charge, localized on the ring structure of the quinoline. Also, note that the ions m/z 129 and 130 only observed in the ESI-MS/MS spectrum and not intermediate in the ESI-MS/MS spectrum are viewed with significant intensity.

Alone or in combination, these characteristic fragmentation processes (loss of hydroxyl groups) are responsible for the majority of the observed fragment ions (Fig. 10). Parent spectra of the major fragment ions typically show either the dehydroxylation ion m/z 146 or the ion m/z 180 their precursor ($m/z = 130$). In order to shed some more light on the model of the overall reaction mechanism, calculations of the Gibbs free energy for the stability of the intermediates. The preferential reaction site for $\bullet$OH in this Fenton process is the position 7 (C7) of the quinoline structure, resulting in an intense fragment corresponding to $m/z = 146$ [27–29]. With this promising lead in hand we next sought to improve the understanding of this reaction.

4. Conclusion

The treatment with dithionite was capable of activating sites in the goethite surface, increasing its methylene blue adsorption capacity as well as that of quinoline. At the same time, the sites created were capable of generating hydroxyl radicals, as indicated by the peroxide decomposition process and also by the oxidation mechanisms of methylene blue and quinoline. In both mechanisms, insertion of hydroxyls in the compound structures suggests the radical nature of the oxidation process. Therefore, the treatment with dithionite represents a simple, relatively economical and effective method for the activation of materials easily found in nature which can be used as catalysts in environmentally relevant processes.

Appendix A. Supplementary data

Supplementary data associated with this article can be found, in the online version, at doi:10.1016/j.molcata.2012.01.005.

References

[1] L.C.A. Oliveira, T.C. Ramalho, D.Q.L. Oliveira, M. Gonçalves, M.C. Pereira, J.D. Fabris, Appl. Catal. B 83 (2008) 169–176.
[2] I.R. Guimaraes, A. Giroto, L.C.A. Oliveira, M.C. Guerreiro, D.Q. Lima, J.D. Fabris, Appl. Catal. B 91 (2009) 581–586.
[3] M. Pera-Titus, V. García-Molina, M.A. Baños, J. Giménez, S. Esplugas, Appl. Catal. B 47 (2004) 219–256.
[4] M. Lu, J. Chen, H. Huang, Chemosphere 46 (2002) 131–136.
[5] R.M. Cornell, U. Schwertmann, The Iron Oxides, 3rd ed., Weinheim-VCH, New York, 2003.
[6] T.R. Gordon, A.L. Marsh, Catal. Lett. 132 (2009) 349–354.
[7] A. Matsumura, T. Kondo, S. Satoa, I. Saito, W.F. Souza, Fuel 84 (2005) 411–416.
[8] S. Das, M.J. Hendry, Appl. Clay Sci. 51 (2011) 192–197.
[9] W. Ferraz, L.C.A. Oliveira, R. Dallago, L. Conceição, Catal. Commun. 8 (2007) 131–134.
[10] E. Neyens, A. Baeyens, J. Hazard. Mater. 98 (2003) 33–50.
[11] L.C.A. Oliveira, J.D. Fabris, R.R.V.A. Rios, W.N. Mussel, R.M. Lago, Appl. Catal. A 259 (2004) 253–259.
[12] L.C.A. Oliveira, M. Gonçalves, M.C. Guerreiro, T.C. Ramalho, J.D. Fabris, M.C. Pereira, K. Sapag, Appl. Catal. A 316 (2007) 117–124.
[13] R.D. Villa, M.R.A. Silva, R.F.P. Nogueira, Quim. Nova 30 (2007) 1799–1803.
[14] R.C.C. Costa, F. Lelis, L.C.A. Oliveira, J.D. Fabris, J.D. Ardisson, R.R.A. Rios, C.N. Silva, R.M. Lago, Catal. Commun. 4 (2003) 525–529.

[15] R.F.P. Nogueira, A.G. Trovó, M.R.A. Silva, R.D. Villa, M. Oliveira, Quim. Nova 30 (2007) 400–408.
[16] O.P. Mehra, M.L. Jackson, Clays Clay Miner. 7 (1960) 317–327.
[17] J.W. Stucki, G.W. Bailey, H. Gan, Appl. Clay Sci. 10 (1996) 417–430.
[18] H. Gan, J.W. Stucki, G.W. Bailey, Clays Clay Miner. 40 (1992) 659–665.
[19] A.S. Anastácio, A. Aouad, P. Sellin, J.D. Fabris, F. Bergaya, J.W. Stucki, Appl. Clay Sci. 39 (2008) 172–179.
[20] A.J. Berry, H.S.C. O'Neill, K.D. Jayasuriya, S.J. Campbell, G.J. Foran, Am. Mineral. 88 (2003) 967–977.
[21] V. Magniena, D.R. Neuvillea, L. Cormierc, B.O. Mysend, V. Brioise, S. Beline, O. Pinetb, P. Richet, Chem. Geol. 213 (2004) 253–263.
[22] L. Galoisy, G. Calas, M.A. Arrio, High-Resolution Chem. Geol. 174 (2001) 307–319.
[23] M. Wilke, G.M. Partzsch, R. Bernhardt, D. Lattard, Chem. Geol. 213 (2004) 71–87.
[24] C.P. Huang, Y.F. Huang, H.P. Cheng, Y.H. Huang, Catal. Commun. 10 (2009) 561–566.
[25] H.H. Huang, M. Lu, J.G.-N. Chen, Water Res. 35 (2001) 2291–2299.
[26] J.W. Stucki, D.C. Golden, C.B. Roth, Clays Clay Miner. 32 (1984) 191–197.
[27] W.F. Souza, I.R. Guimaraes, M.C. Guerreiro, L.C.A. Oliveira, Appl. Catal. A 360 (2009) 205–209.
[28] W.F. Souza, I.R. Guimaraes, D.Q. Lima, C.L.T. Silva, L.C.A. Oliveira, Energy Fuels 23 (2009) 4426–4430.
[29] I.R. Guimaraesa, L.C.A. Oliveira, P.F. Queiroz, T.C. Ramalho, M. Pereira, J.D. Fabris, J.D. Ardisson, Appl. Catal. A 347 (2008) 89–93.